Electrospray Steady-State and Transient Emission Behavior

IEPC-2019-368

Presented at the 36th International Electric Propulsion Conference
University of Vienna • Vienna, Austria
September 15-20, 2019

Nolan M. Uchizono[1], Adam L. Collins[2], Anirudh Thuppul[3], Peter L. Wright[4]
University of California, Los Angeles, California, 90095, United States of America

Daniel Q. Eckhardt[5]
Air Force Research Laboratory, RQRS, Edwards AFB, California, 93401, United States of America

John K. Ziemer[6]
NASA Jet Propulsion Laboratory, California Institute of Technology, Pasadena, CA, 91109, USA
University of California, Los Angeles, California, 90095, United States of America

and

Richard E. Wirz[7]
University of California, Los Angeles, California, 90095, United States of America

Abstract: The UCLA Plasma & Space Propulsion Lab is using both high-speed microscopy and emitter current measurements to provide insight into the electrohydrodynamics of electrospray emission processes. Test are being performed via benchtop testing of low-conductivity ethanol and *in vacuo* testing of high-conductivity ionic propellant (EMI-Im). The physical deformation of the liquid meniscus and angle of the cone-jet with respect to the emitter/extractor axis is observed over a range of flow rates and extractor voltages. The results of this study indicate that EMI-Im electrosprays are stable over a very wide range of setpoints, in comparison to lower-conductivity propellants, but exhibit off-axis asymmetries that must be considered for thruster life and performance. Furthermore, under certain conditions, transient instabilities occur during startup and shutdown that must be consider for thruster operation and lifetime.

Nomenclature

β	=	ratio of charge contained by a droplet to its Rayleigh limit charge
γ	=	surface tension [N/m]
d_n	=	capillary inner diameter [m]
ε	=	dielectric constant
E	=	nominal electric field ($E = V_e/S$) [V/m]
f_{cj}	=	choked-jet pulsation frequency [Hz]

[1] PhD Student, Mechanical and Aerospace Engineering Department, nuchizono@ucla.edu
[2] Research Scientist, Mechanical and Aerospace Engineering Department, collinsalc55@ucla.edu
[3] PhD Student, Mechanical and Aerospace Engineering Department, athuppul@ucla.edu
[4] PhD Student, Mechanical and Aerospace Engineering Department, plloydwright@ucla.edu
[5] Group Lead, AFRL/RQRS, daniel.eckhardt.3@us.af.mil
[6] LISA Microthruster Technology Lead, AIAA Senior Member, john.k.ziemer@jpl.nasa.gov
[7] Professor, Mechanical and Aerospace Engineering Department, wirz@ucla.edu

f_{oc}	=	oscillating cone pulsation frequency [Hz]
θ_c	=	angle between the apex of the cone-jet and the center axis of the emitter [degrees]
I	=	emitter current [A]
κ	=	conductivity [S/m]
L	=	emitter length [m]
μ	=	viscosity [N-s/m]
Q_m	=	minimum flow rate [L/s]
Q_s	=	supplied flow rate [L/s]
ρ	=	density [kg/m^3]
r_c	=	radius of curvature of the meniscus during the relaxation phase of pulsation [m]
Re	=	Reynolds number
S	=	separation distance between emitter and extractor [m]
V_m	=	minimum emission voltage [V]
V_e	=	emitter bias voltage [V]

I. Introduction

A key contributing factor to lifetime reduction of electrospray thrusters is propellant flux to the extractor and accelerator grids [1]. Emission stability has been identified as an important process leading to grid impingement [2]. Therefore, understanding electrospray emission stability is critical to improving the lifetime of electrospray propulsion devices. The two studies presented in this paper represent efforts to characterize emission instabilities relevant to electrospray thruster lifetime. The objective of the first study is to demonstrate that observed instabilities in the cone-jet propagate into the current drawn by the emitter, suggesting the use of emitter current as a diagnostic for electrospray stability. The objective of the second study is to build off of the work presented by Wright, Thuppul, and Wirz [2] by performing similar emission stability experiments on an ionic liquid propellant (EMI-Im).

II. Background

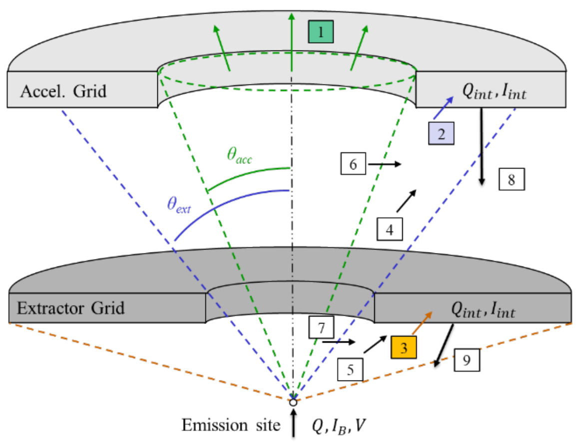

Figure 1. Diagram describing propellant fluxes in an electrospray thruster *[4]***.** *Most emitted propellant exits the device through the accelerator grid (1). Thruster lifetime is decreased by emitted propellant impinging on the accelerator grid (2) and extractor grid (3), which is caused by off-axis emission (4 and 5) and plume expansion (6 and 7).*

A. Electrospray Lifetime

The most likely limitation to thruster life is the impingement of emitted propellant onto the extraction and acceleration grids [3] [4]. Figure 1 shows the two mechanisms that contribute to grid impingement: plume expansion and off-axis emission. Plume expansion results from droplet interactions downstream of the emission site [5]. Off-axis emission originates from the emission site, where droplets are ejected at high angles with respect to the capillary axis. While stable off-axis emission can be detrimental to thruster lifetime [4] [6] [7], the emphasis of the presented study is placed on temporally unstable modes.

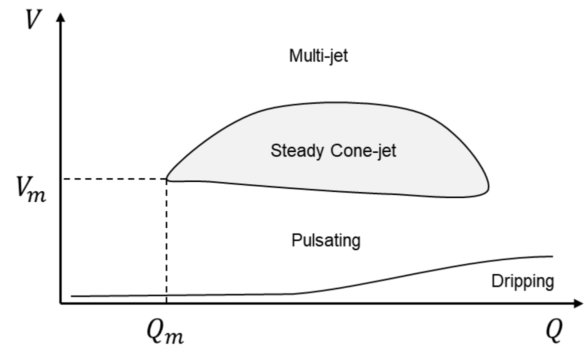

Figure 2. Flow map for a general electrospray device, adapted from Cloupeau and Ramos by Wright, Thuppul, and Wirz.

B. Instabilities in Electrosprays

Electrospray emission modes are often represented on a stability map, with modes plotted as a function of applied voltage and flow rate [8] [2], as shown in Figure 2. Electrospray emission is categorized into four different modes: (1) steady cone-jet, (2) multi-jet, (3) pulsating, and (4) whipping. Steady cone-jet is the desired operating mode for electrospray propulsion devices. Devices operating in multi-jet mode may exhibit stable thrust, but the highly off-axis emission profile drastically limits electrospray thruster lifetime. Unstable pulsating and whipping modes are the subject of extensive analysis in the electrospray community due to their applicability in aerosol physics, electrospray ionization, and electrospinning [9]. Axisymmetric instabilities, such as pulsating mode, result in a nonuniform distribution of droplet velocities, which may lead to plume expansion through coulombic interactions. The non-axisymmetric "whipping mode" instability results in significant off-axis emission. Characterizing the dominant emission instabilities of EMI-Im will provide insight into the two primary contributions to beam impingement on the grids, and is therefore critical to predicting the lifetime of colloid thrusters.

The pulsating (or "intermittent") cone-jet is an axisymmetric instability that can be divided into two regimes. The first pulsation regime, often referred to as the "choked-jet" mode, occurs when the supplied flow rate, Q_s is less than a minimum flow rate, Q_m, and the emitter bias voltage, V_e is greater than the minimum extraction voltage, V_m [10] [11] [12]. Choked-jet pulsation behavior is dictated by the imbalance of flow supplied to the cone and emitted by the jet. Due to the elevated conductivity of EMI-Im the charge relaxation time ($\tau = \varepsilon\varepsilon_0/\kappa$) is on the order of 100 ps. Chen *et al*. [11] showed that choked-jet pulsation frequency scales as:

$$f_{cj} \propto \frac{\kappa E^2}{\varepsilon \mu L}\left(\frac{\rho d_n^5}{\gamma}\right)^{1/2} \quad (1)$$

Where κ is conductivity, E is the nominal electric field, ε is the dielectric constant, μ is viscosity, ρ is density, γ is surface tension, and d_n is the inner diameter of the capillary. Inserting the emitter dimensions and fluid properties for EMI-Im in Eq. (1), the pulsation frequency is found to be on the order of 10 MHz. Responses at the 10 MHz level exceed the current capability of our diagnostics, so choked-jet pulsation was not expected to be resolved in this experiment.

The second pulsation regime, known as the "oscillating cone" mode, occurs when Q_s is greater than Q_m and V_e is less than V_m [13] [14]. Oscillating cone behavior is dictated by free oscillation of the meniscus. Marginean *et al.* [14] derived a relationship between the oscillating cone pulsation frequency and the Rayleigh limit charge fraction:

$$f_{oc} = \sqrt{\frac{2\gamma(1-\beta^2)}{\pi^2 \rho r_c^3}} \quad (2)$$

Where r_c is the radius of the cone's apex during the relaxation period of pulsation. Assuming the apex diameter falls between the capillary's inner and outer diameter (70 µm to 290 µm), the pulsation frequency can be estimated over a range of β. Figure 3 shows that the pulsation frequency will be less than 10 kHz, which is well within the range of our imaging capabilities.

The linear stability analysis conducted by Hohman *et al.* [15] suggests the existence of three types of instabilities in electrified jets: Rayleigh mode, conducting mode, and whipping mode. The "Rayleigh" mode is analogous to the classical axisymmetric Rayleigh instabilities that describe the breakup of a jet of liquid into droplets. The "conducting" mode is an axisymmetric instability analogous to the Rayleigh mode, but owing more to perturbations in surface charge density, rather than surface tension. The "whipping" mode is a non-axisymmetric instability that manifests due to repulsion of surface charge along the jet.

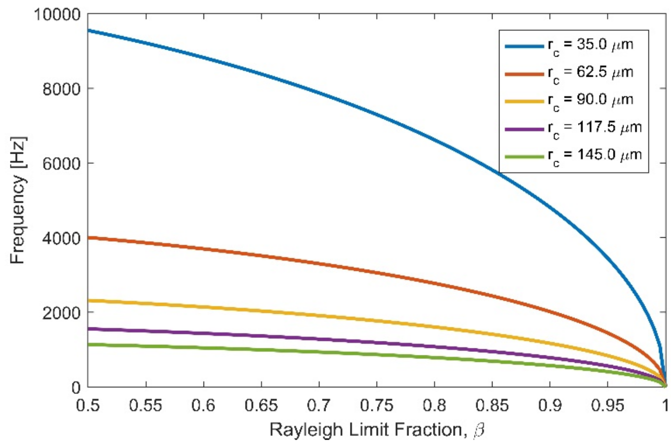

Figure 3. Pulsation frequency estimates when operating in the oscillating cone mode. *Five different meniscus curvature radii were chosen between the inner and outer radius of the capillary used in the EMI-Im experiment.*

To date, electrospray stability experiments have exclusively focused on low-conductivity fluids (κ ~ 10^{-5} S/m) [2] [16] [17] [18]**.** Hohman's linear stability analysis of electrospray emission has shown that the conductivity and viscosity of the fluid have a strong effect on the growth rate of instabilities in electrospray systems. The viscosity and conductivity of EMI-Im (~30 N-s/m [19] and ~1 S/m [20]) are orders of magnitude greater than fluids investigated in previous stability experiments, so emission behavior is expected to be substantially different.

III. Coupled High-Speed Microscopy and Current Measurements of an Ethanol Electrospray

The objective of the first effort was to use coupled high-speed current and microscopy to assess how effectively current measurements can serve as a diagnostic for emission behavior in the absence of high-speed microscopy. Emitter current has been previously demonstrated as an effective measure of electrospray stability and compares very well to images of the emission site [16] [17] [18]. High-speed current measurements may improve fidelity of emission stability experiments by serving as a complementary diagnostic to high-speed microscopy, or serve as a stand-alone stability diagnostic when imaging the emission site is not possible. A relatively low conductivity propellant (i.e., pure ethanol) was used to provide manageable emission frequencies and feature sizes that can be relatively easily observed via the high-speed microscopy. For ease of prototyping, the benchtop ethanol electrospray setup used in the

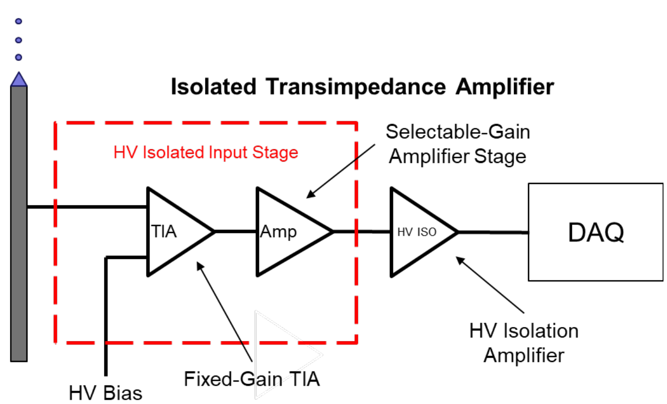

Figure 4. Schematic diagram for the coupled high-speed microscopy and emitter current measurement experiment.

experiments reported by Wright, Thuppul, and Wirz [2] was leveraged for development of a high-speed transimpedance amplifier (TIA).

A. Experiment Setup

Tests are conducted in the Plasma & Space Propulsion Laboratory (PSPL) at UCLA [21]. An experiment test apparatus called the Atmospheric Pressure Electrospray eXperiment (APEX) was developed for benchtop studies of electrospray phenomena. A pressure-driven flow system fed ethanol to a 34 gauge, tapered, stainless-steel capillary emitter. The capillary was biased to 1.4 kV with respect to a grounded extractor. The configuration used to energize the emitter and measure its current is shown in Figure 4. Prior studies used a biased extractor with a grounded emitter, and so emitter current measurements were relatively trivial. However, electrospray propulsion devices instead require biasing the emitter to high voltages with respect to the grounded extractor to produce thrust. Therefore, all current measurements must be obtained with an electrically isolated current transducer. A high-speed camera was used to image the emission site at a framerate of 210 kHz, and was synchronized to a data acquisition system that recorded the TIA output.

B. Results and Discussion: High-Speed Current Measurement Experiment

A single voltage sweep from 1 kV and 1.4 kV with 100 V steps was performed at approximately 1000 pL/s. To assess the stability of emission, the dimension of the high-speed videos was reduced by taking the aggregate pixel intensity of each image. The power spectral density (PSD) was obtained using the resulting time-domain pixel intensity signal, $Y_i(t)$. The PSDs of the unstable modes shown in Figure 5 and Figure 6 reveal characteristic oscillations that agree very well with pulsating emission observed in the videos. The emitter current PSD also agrees very well with the pixel intensity signal. As emitter bias voltage increases from 1.1 kV to 1.4 kV, the pulsation frequency increases from ~1.5 kHz to ~4.1 kHz. The observed trend between frequency and emitter voltage agrees with the frequency scaling for choked-jet pulsation, as shown in Eq. (1). The peaks and valleys in the emitter current oscillations map directly to the emission and relaxation phases of the pulsation mode. The results of the coupled current and microscopy experiment validate the feasibility of using emitter current measurements to classify emission mode.

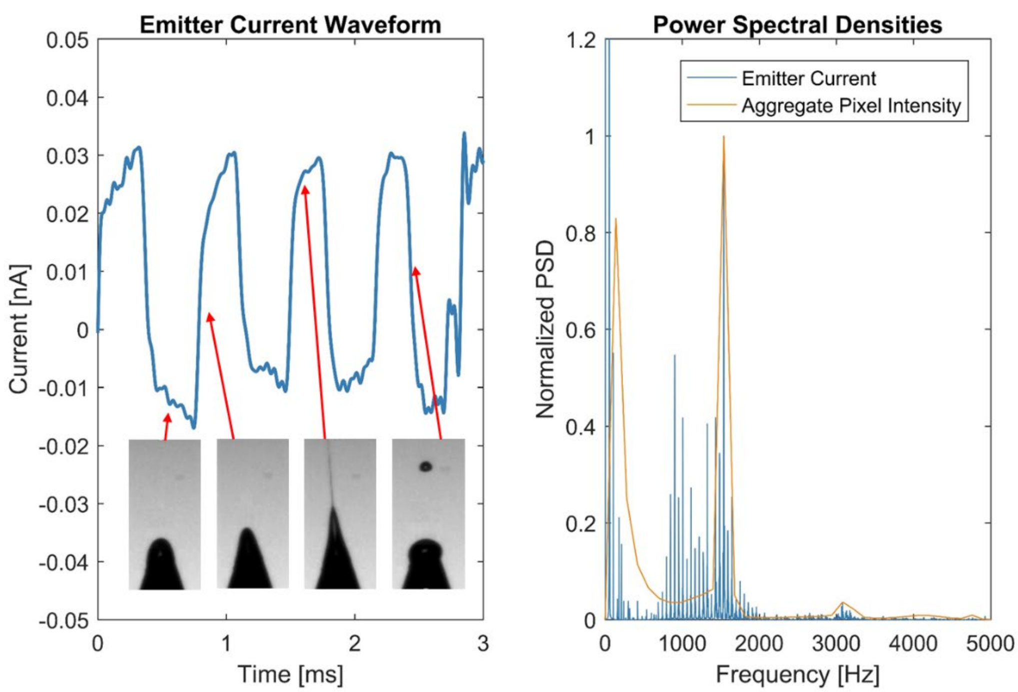

Figure 5. Current and video data of a pulsating ethanol electrospray operating at 1000 pL/s flow rate and 1.1 kV extraction voltage. *The left image shows the time-domain current waveform with corresponding images at different phases in the pulsation cycle. The right image shows the PSD of the emitter current and the aggregate pixel intensity per frame. The characteristic pulsation frequency appears as a peak at approximately 1.5 kHz in both sets of data.*

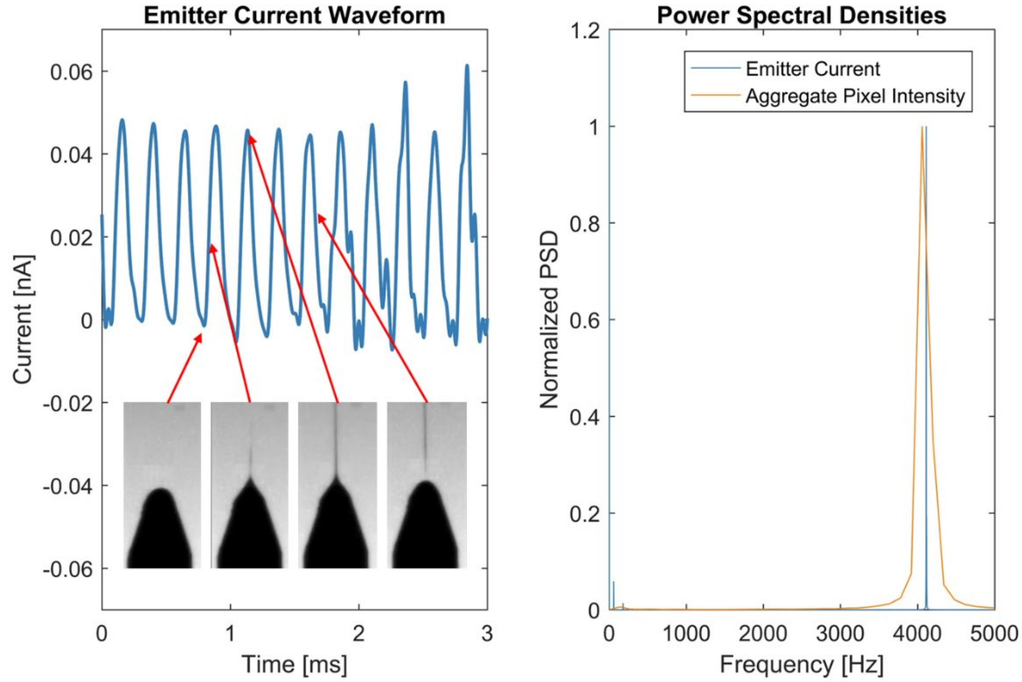

Figure 6. Current and video data of a pulsating ethanol electrospray operating at 1000 pL/s flow rate and 1.4 kV extraction voltage. *The left image shows the time-domain current waveform with corresponding images at different phases in the pulsation cycle. The right image shows the PSD of the emitter current and the aggregate pixel intensity per frame. The characteristic pulsation frequency appears as a peak at approximately 4.1 kHz in both sets of data.*

IV. EMI-Im Electrospray Stability Experiment

While ethanol electrosprays serve as excellent canonical devices for validating diagnostics concepts, studying behavior of electrosprays operating with highly-conductive propellants (i.e., EMI-Im) is ultimately necessary to draw relevance to electrospray propulsion. Two stability experiment campaigns were performed: a stability mapping campaign, and a transient emission campaign.

A. Experiment Setup

The UCLA Plasma & Space Propulsion Lab has developed the Highly Optimizable Apparatus for Groundbreaking Investigation of Electrosprays (HOAGIE) as a testbed to study the dynamics and lifetime of electrospray thrusters [1]. Propellant flow was controlled by a pressure-over-fluid feed system, where an isolated reservoir was pressurized with dry nitrogen using mass flow controllers to achieve precise flow rates. The EMI-Im propellant was conditioned by exposure to low vacuum for at least 24 hours prior to experiment operations to ensure negligible water and gas content. A high-voltage bias was applied to the emitter with respect to the grounded extractor grid. The emitter used in this experiment was a chamfered platinum emitter, with an extractor geometry identical to that used in the DRS ST-7 mission. For the presented studies, a 2 MHz high-speed camera was used in conjunction with a long-distance microscope (LDM) optical system developed in-house to observe deformations to the emitter's liquid meniscus as a function of flow rate and voltage. The camera was operated at 210 kHz for the presented experiments.

The stability map was obtained by taking high-speed videos while parametrically sweeping the emitter bias voltage and propellant flow rates. Flow was operated from 400 to 1300 pL/s in 300 pL/s steps, while voltage was swept from 1.3 kV to 2.0 kV in 100 V steps at each flow setpoint. Flow rates were chosen to match nominal operating setpoints. Voltages were chosen between the minimum voltage required for emission, and the maximum voltage output of the power supply. Transient stability tests were performed by obtaining measurements during startup and shutdown of emission, which can be commanded through nominal or off-nominal application of control setpoints. Nominal conditions involve maintaining the applied voltage bias while ramping flow up or down. Off-nominal conditions involve rapidly applying or removing voltage while maintaining constant flow.

B. Results and Discussion: Stability Mapping Campaign

No pulsating, whipping, or multi-jet instabilities were observed in the emission stability experiment – the emission appeared to reside exclusively in the stable cone-jet regime. However, as voltage was varied, the cone-jet appeared to tilt off to the side, particularly at elevated voltages. In lieu of a traditional stability map, the angle of the cone's apex with respect to the center axis of the emitter, θ_c has been plotted against the emitter voltage in Figure 7. θ_c appears to have a strong dependence on the emitter voltage, with the highest off-axis emission occurring at the upper bound of voltage setpoints. Off-axis emission appears to be negligible between 1.5 and 1.7 kV, which is notable as the nominal extraction voltage bias is 1.6 kV. The lack of an apparent dependence on flow is significant, as thrust is controlled by changing flow rate. Therefore, at a fixed extraction voltage, a colloid thruster should not experience off-axis emission over its nominal flow ranges. While stable off-axis emission is extremely important when considering electrospray lifetime, the focus of this study is temporal instabilities in the emission process. The observed stable off-axis emission warrants further study. Images of the emitter at each setpoint are shown in Figure 8.

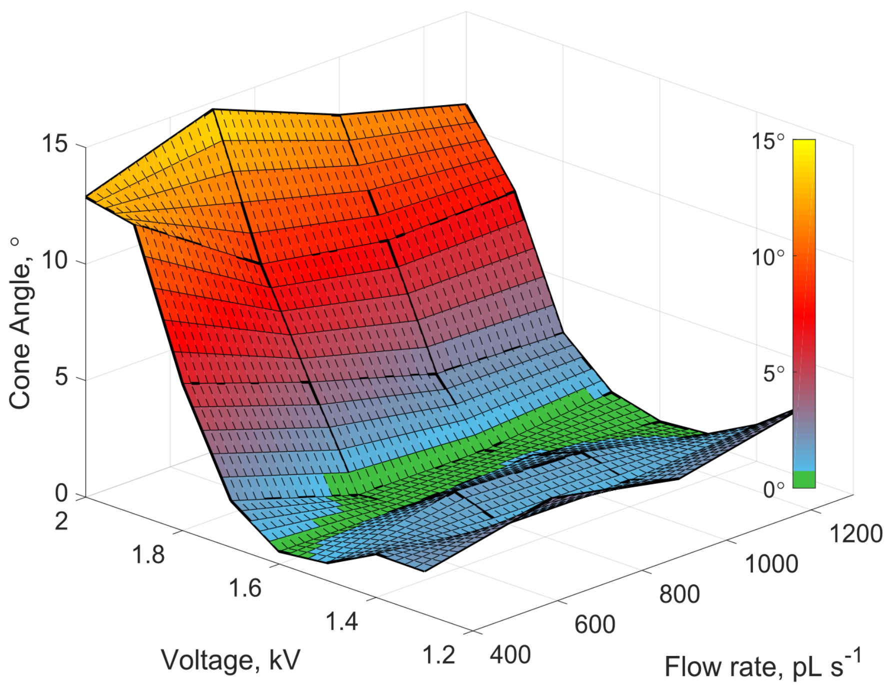

Figure 7. Parameter map of cone-jet emission angle for an EMI-Im electrospray. *No temporal instabilities were observed over the entire flow-voltage map, so emission "stability" has instead been characterized based on the cone-jet's emission angle with respect to the center axis, θ_c.*

The range of emission setpoints performed in the presented experiment exceed the parameters used in the ethanol stability experiments reported by Wright, Thuppul, and Wirz [2]. When compared to ethanol, the "stability island" for EMI-Im stable cone-jet emission appears to be much larger than that of ethanol in steady-state operation. Increased stability of EMI-Im electrosprays can likely be attributed to the high viscosity and conductivity of EMI-Im.

Toroidal and helical flow patterns have been previously observed and studied in Taylor cones [22] [23]. Toroidal flow patterns driven by electrical shear stresses at the cone surface are always present in electrospray emission. However, helical motion is the result of azimuthal instabilities, whose growth rates depend on viscosity and conductivity of the fluid. Barrero *et al.* [24] analytically derived a relationship for local fluid velocity induced by interfacial electrical stresses for a flow pattern that exhibits no helical motion:

$$U \sim \left[\frac{\gamma \varepsilon_0 I^2}{d_n^3 \kappa^2 \mu^2}\right]^{\frac{1}{2}} \tag{3}$$

Where *I* is the emitter current. Reynolds number is then given by:

$$Re = \frac{\rho U d_n}{\mu} = \left[\frac{\gamma \varepsilon_0 \rho^2 I^2}{d_n K^2 \mu^4}\right]^{\frac{1}{2}} \tag{4}$$

For a purely toroidal flow pattern, *Re* must be less than, or on the order of, unity [24]. In the presented EMI-Im stability experiments, *Re* was found to be approximately 10^{-5} for all setpoints. By contrast, the ethanol stability experiments reported by Wright, Thuppul, and Wirz [2] yielded *Re* of approximately 10^2. The whipping motion observed at elevated extraction voltages in ethanol electrosprays may simply be a superposition of off-axis emission with a helical flow pattern in the cone. With EMI-Im, where the helical motion is suppressed, only steady off-axis emission arises.

Hohmann *et al*. [15] discuss the effect of viscosity on the growth rate of instabilities in electrified jets, noting that even small increases in viscosity of a fluid will act to push the most unstable wavelength into the long-wavelength regimes. Nayak *et al.* [25] also experimentally observed that decreasing the viscosity of a working fluid decreases the stability of the jet.

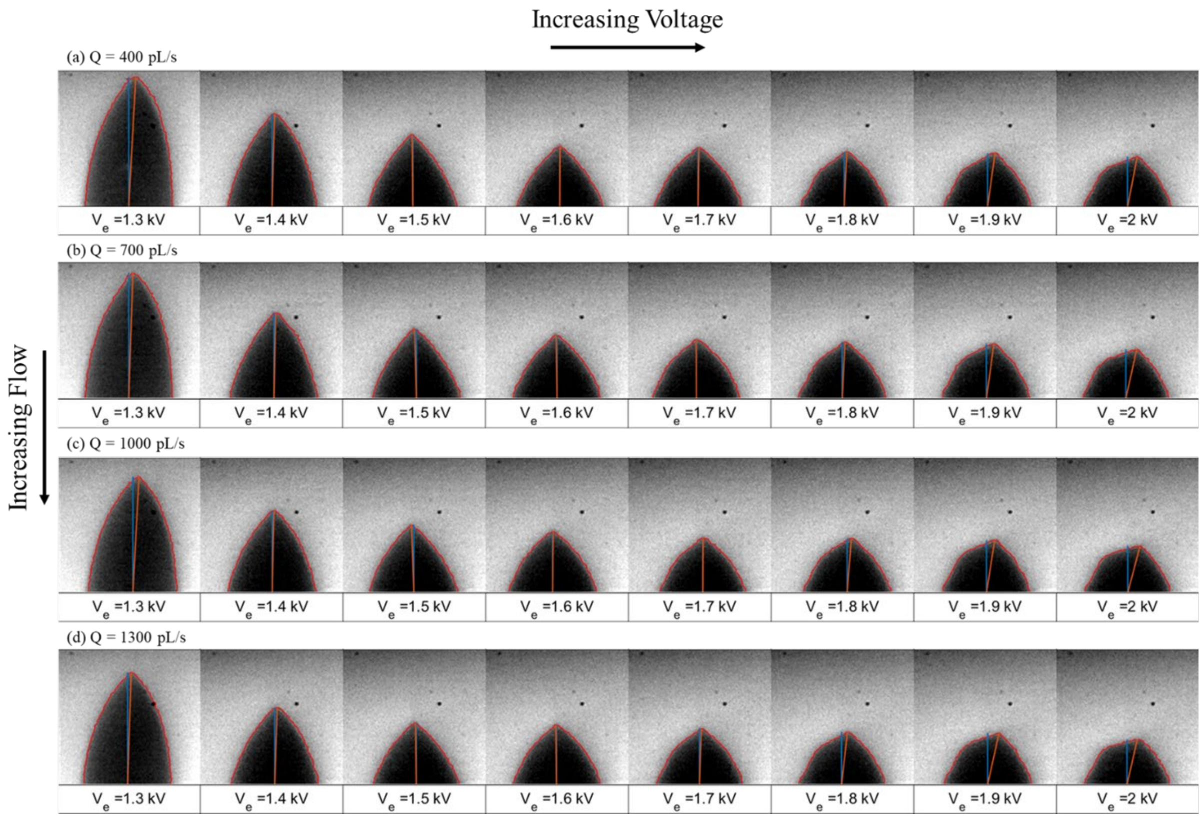

Figure 8. Images of EMI-Im electrospray emission with flow setpoints between 400 pL/s and 1300 pL/s, and from 1.3 kV to 2.0 kV. *The blue line indicates the center axis of the capillary. The orange line indicates the angle of the cone's apex with respect to the center axis. Image labels corresponding to the following flow rates: (a) 400 pL/s, (b) 700 pL/s, (c) 1000 pL/s, and (d) 1300 pL/s.*

C. Results and Discussion: Transient Emission Campaign

Nominal-condition startup results are shown in Figure 9(a). As propellant flows from the capillary, the resulting droplet deforms into a conical shape due to the applied electric field. Eventually, the droplet height reaches a point where the stresses at the tip permit formation of a cone-jet. A slight overshoot in cone height is observed during the emission-onset transient. The emission reaches a steady cone-jet mode approximately 150 µs after the onset of emission.

Nominal shutdown results are shown in Figure 9(b). When flow is cut off to the emitter, the jet continues to extract propellant from the cone until the volume can no longer sustain emission. The jet ceases emission within 375 µs, but the meniscus continues to recede over the next 1-2 ms. Off-nominal shutdown shown in Figure 9(c) appeared to behave identically to the nominal shutdown case, where shutdown occurred as the bias voltage was removed. The

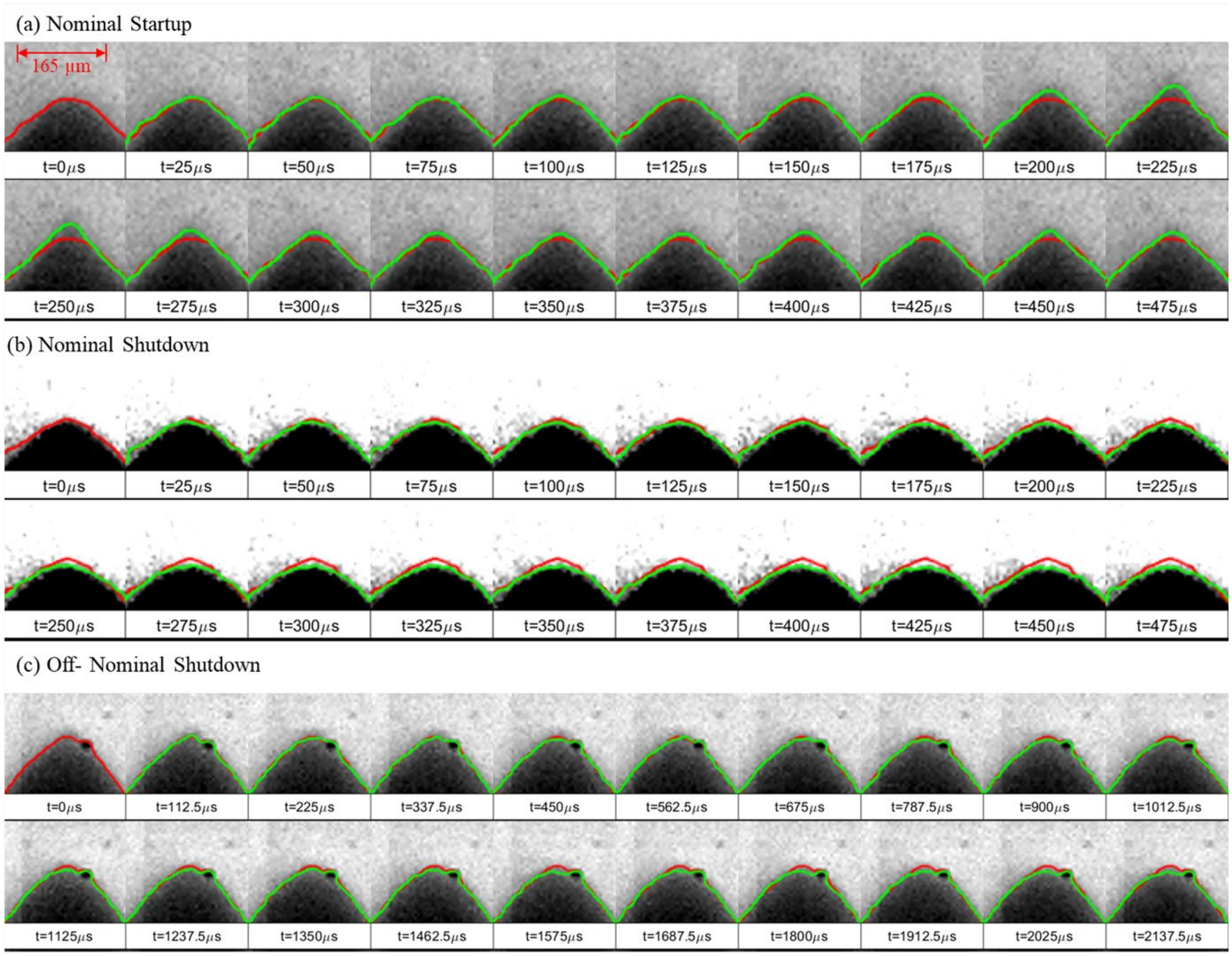

Figure 9. Transient stability test image sequences. *The red line represents the initial edge of the meniscus, and is plotted in each subsequent frame as a reference. The green line represents the instantaneous meniscus edge. (a) Nominal operation startup transient, 0 to 400 pL/s, 1.6 kV emitter bias. (b) Nominal operation shutdown transient, 400 to 0 pL/s, 1.6 kV emitter bias. (c) Off-nominal operation shutdown, 1300 pL/s, 1.6 kV to 0 kV emitter bias.*

operating conditions during nominal startup and shutdown should traverse the region of the stability map that typically enables choked-jet pulsation, yet no pulsation was observed during the test campaign. It's possible that choked-jet pulsation occurs at significantly higher frequencies than the camera can resolve, and that a brief period of pulsating instability occurs during the nominal startup/shutdown transients. A lower bound of 200 kHz on any pulsation frequency during the startup transient is concluded.

Off-nominal startup exhibited extremely unstable behavior. Due to the constant flow of propellant to the emitter prior to application of a bias voltage, a large droplet of propellant had accumulated on the side of the emitter. Images of the off-nominal onset of emission are shown in Figure 10(a). When the extraction voltage was turned on, an off-axis cone-jet formed at the apex of the meniscus. Approximately 10 ms after the off-axis cone-jet began, a larger secondary droplet emerged from the reservoir of excess propellant. Approximately 5 ms later, the secondary droplet merged with the primary emission cone and began pulsating.

After the onset of emission, axisymmetric pulsating and non-axisymmetric whipping instabilities were observed. Figure 10(b) shows a single cycle of pulsation. Figure 10(c) shows an image sequence isolating the whipping instability that grew in oscillating frequency during the relaxation phase of the pulsation cycle. The whipping instabilities clearly cause significant off-axis emission, and a spray of macroscopic droplets were observed as the jet

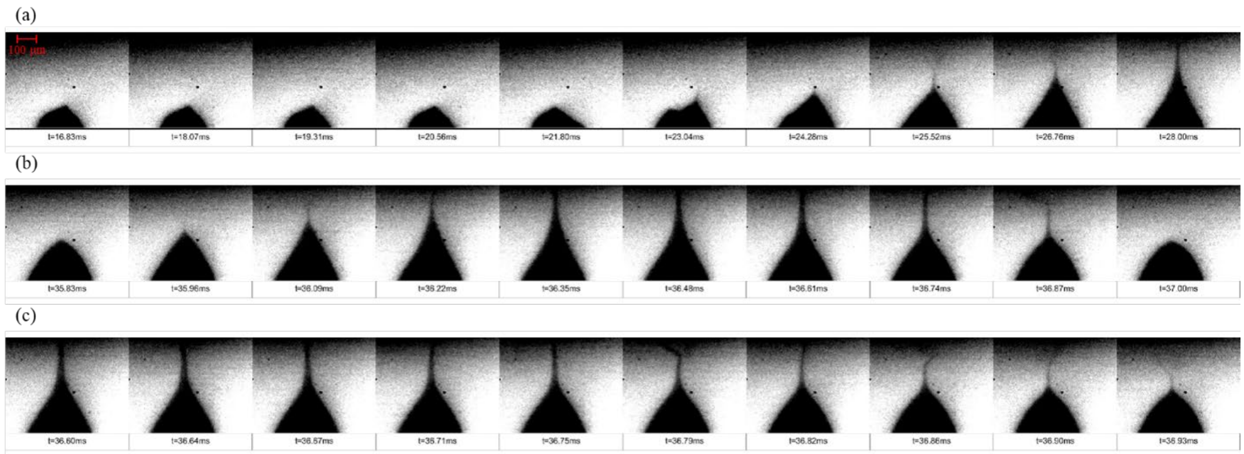

Figure 10. Off-nominal operation startup image sequences, 1300 pL/s flow, 0 kV to 1.6 kV emitter bias. *(a) Onset of emission transient. Two cones merge into a single emission site that immediately begins pulsating. (b) Single cycle of pulsation after onset of emission. (c) Whipping instability that occurs during relaxation period of the pulsation cycle.*

retracted. The scale of these images was found to be ~3.76 µm/pixel, so the observed droplets must be on the order of 0.1 – 1 µm. The time and frequency-domain representations of aggregate pixel intensity, $Y_i(t)$ for the off-nominal startup video is shown in Figure 11. The strong peak at <100 Hz corresponds to the vibration of the camera and chamber. A frequency band from 0.5 – 2.5 kHz corresponds to the pulsating and whipping instabilities.

Figure 12 shows a spectrogram of the pixel intensity signal that was generated using a 5000 bin triangle window with a 4900 sample overlap. The spectrogram shows a ~1 kHz pulsation that begins at the onset of emission at around 23 ms, and varies by ~290 Hz over time. The bands greater than 1 kHz correspond to harmonics of the pulsating emission. Due to negligible hydraulic resistance of the accumulated propellant on the emitter, the effective flow rate is very high. The observed frequencies are on the order of estimated values for oscillating cone pulsation plotted in Figure 3. High effective flow rate also meets the conditions necessary for oscillating cone pulsation, but the voltage bias (1.6 kV) is much higher than the minimum extraction voltage. The discrepancy between the conditions expected to produce oscillating cone pulsation and those used in the experiment merits further study. The pulsation eventually damps out after several hundred milliseconds as the accumulated propellant is cleared, but the record length of the camera was insufficient to capture the transition to stability. Future experiments will extend the record length to accommodate the complete transient unstable period.

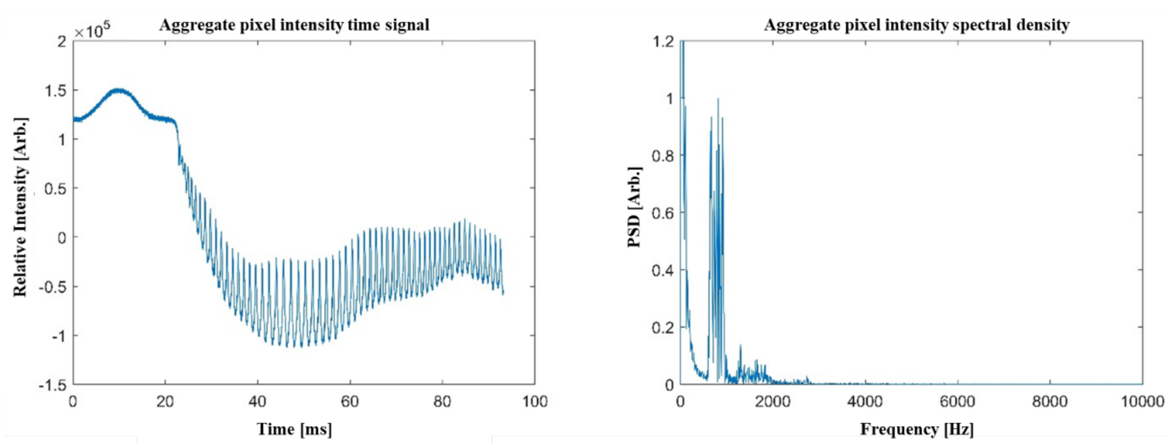

Figure 11. Time and frequency domain representations of aggregate pixel intensity for the video of an EMI-Im electrospray during off-nominal startup.

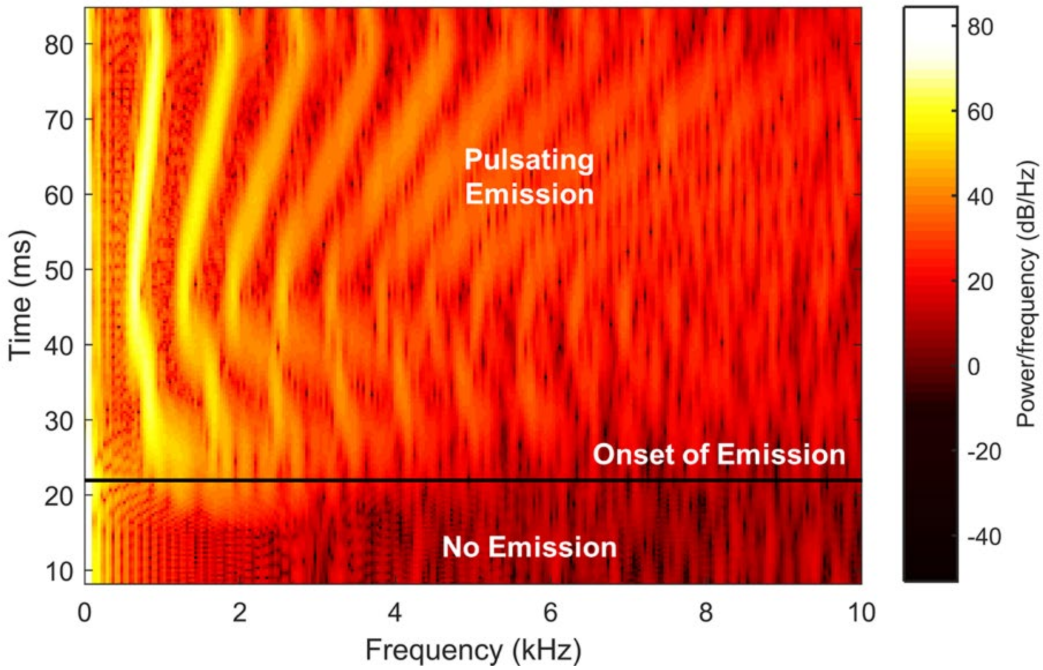

Figure 12. Narrowband spectrogram of aggregate pixel intensity for the video of an EMI-Im electrospray during off-nominal startup. *The approximately 100 Hz frequency bands correspond to vibration of the setup. Onset of emission is denoted by the horizontal black line at approximately 22 ms. The 1 kHz band corresponds to the pulsation characteristic frequency. Bands above 1 kHz are harmonics of the pulsation band. The pulsation band appears to deviate by approximately 290 Hz over time.*

V.Conclusion

Assessing electrospray emission stability is critical to estimating the lifetime of electrospray thrusters. Preliminary results of coupled high-speed microscopy and current measurements of a pulsating ethanol electrospray demonstrate the ability to characterize emission stability based on current. The results of an experiment assessing the stability of an EMI-Im electrospray show steady cone-jet emission across the entire parameter space. However, certain operating points exhibit significant off-axis emission. Highly off-axis stable cone-jet modes were observed to occur at elevated voltages (1.8 kV – 2.0 kV). During nominal startup and shutdown conditions, a steady cone-jet emerges and undergoes a slight overshoot, settling to a steady height after approximately 150 µs. During off-nominal shutdown conditions, the steady cone-jet is extinguished within 375 µs. Off-nominal startup exhibits extremely unstable emission, with both pulsating-cone and whipping-jet instabilities present. Unstable behavior during off-nominal startup is likely attributed to the accumulation of excess propellant on the side of the capillary. The hydraulic resistance of a stagnant droplet is negligible, so it can produce an arbitrarily high flow rate when the bias voltage is applied. Future work will involve investigating stable off-axis emission modes by characterizing the ranges of off-axis emission that result in grid impingement. Improved imaging and current diagnostics are being developed at UCLA to study the high frequency (~10 MHz) choked-jet pulsating modes that may occur in certain emission regimes. Furthermore, the high-speed current transducer will be integrated into the experiments as an additional diagnostic for evaluating emission stability.

Acknowledgments

The authors would like to thank Collene Marrese-Reading from NASA JPL, Daniel Courtney and Nathaniel Demmons from Busek, and Michael Natisin from AFRL for their insights. The authors would also like to thank undergraduate researchers Tim Simka and Josue Castillo for their efforts in helping perform experiments. This work was funded by the Air Force Research Laboratory, and by a grant from NASA/JPL award no. 1580267:3.

VI.References

[1] R. E. Wirz, A. L. Collins, A. Thuppul, P. L. Wright, N. M. Uchizono, H. Huh, M. J. Davis, J. K. Ziemer and N. R. Demmons, "Electrospray Thruster Performance and Lifetime Investigation for the LISA Mission," in *AIAA 2019-3816, 2019 Propulsion and Energy Forum*, Indianapolis, IN, 2019.

[2] P. L. Wright, A. Thuppul and R. E. Wirz, "Life-Limiting Emission Modes for Electrospray Thrusters," in *AIAA 2018-4726.c1, 54th AIAA/ASME/SAE/ASEE Joint Propulsion Conference & Exhibit*, Cincinnati, OH, 2018.

[3] J. Ziemer, C. Marrese-Reading, C. Dunn, A. Romero-Wolf, C. Cutler, S. Javidnia, T. Li, I. Li, G. Franklin, P. Barela and et al., "Colloid Microthruster Flight Performance Results from Space Technology 7 Disturbance Reduction System," in *IEPC-2017-578, 35th International Electric Propulsion Conference*, Atlanta, GA, 2017.

[4] A. Thuppul, P. L. Wright and R. E. Wirz, "Lifetime Considerations and Estimation for Electrospray," in *AIAA 2018-4652, 54th AIAA/ASME/SAE/ASEE Joint Propulsion Conference & Exhibit*, Cincinnati, OH, 2018.

[5] M. Davis, H. Huh, A. L. Collins and R. E. Wirz, "Electrospray Plume Evolution Via Discrete Simulations," in *IEPC-2019-590, 36th International Electric Propulsion Conference*, Vienna, Austria, 2019.

[6] A. Thuppul, P. L. Wright, N. M. Uchizono, A. L. Collins and R. E. Wirz, "Spatially-Resolved Mass Flux and Current Measurements for Electrospray Plumes," in *IEPC-2019-571, 36th International Electric Propulsion Conference*, Vienna, Austria, 2019.

[7] A. L. Collins, A. Thuppul, P. L. Wright, N. M. Uchizono, H. Huh, M. Davis and R. E. Wirz, "Assessment of Grid Impingement for Electrospray Thruster Lifetime," in *IEPC-2019-213, 36th International Electric Propulsion Conference*, Vienna, Austria, 2019.

[8] M. Cloupeau and B. Prunet-Foch, "Electrostatic spraying of liquids in cone-jet mode," *Journal of Electrostatics,* vol. 22, no. 2, pp. 135-159, 1989.

[9] J. Rosell-Llompart, J. Grifoll and I. G. Loscertales, "Electrosprays in the cone-jet mode: From Taylor cone formation to spray development," *Journal of Aerosol Science,* vol. 125, pp. 2-31, 2018.

[10] J. De La Mora, "On the Outcome of the Coulombic Fission of a Charged Isolated Drop," *Journal of Colloid and Interface Science,* vol. 178, no. 0109, pp. 209-218, 1996.

[11] C.-H. Chen, D. A. Saville and I. A. Aksay, "Scaling laws for pulsed electrohydrodynamic drop formation," *Applied Physics Letters,* vol. 89, no. 124103, 2006.

[12] D. B. Bober and C.-H. Chen, "Pulsating electrohydrodynamic cone-jets: from choked jet to oscillating cone," *Journal of Fluid Mechanics,* vol. 689, pp. 552-563, 2011.

[13] L. Rayleigh, "On the equilibrium of liquid conducting masses charged with electricity," *The Philosophical Magazine,* vol. 14, pp. 184-186, 1882.

[14] I. Marginean, P. Nemes, L. Parvin and A. Vertes, "How much charge is there on a pulsating Taylor cone?," *Applied Physics Letters,* vol. 89, no. 064104, 2006.

[15] M. M. Hohman, M. Shin, G. Rutledge and M. P. Brenner, "Electrospinning and electrically forced jets. I. Stability theory," *Physics of Fluids,* vol. 13, no. 2201, 2001.

[16] R. Juraschek and F. Rollgen, "Pulsation phenomena during electrospray ionization," *International journal of mass spectrometry,* vol. 177, no. 1, pp. 1-15, 1998.

[17] P. Nemes, I. Marginean and A. Vertes, "Spraying Mode Effect on Droplet Formation and Ion Chemistry in Electrosprays," *Analytical Chemistry,* vol. 79, pp. 3105-3116, 2007.

[18] S. Verdoold, L. L. F. Agostinho, C. U. Yurteri and J. C. M. Marijnissen, "A generic electrospray classification," *Journal of Aerosol Science,* vol. 67, pp. 87-103, 2014.

[19] H. Tokuda, K. Hayamizu, K. Ishii, M. A. B. H. Susan and M. Watanabe, "Physiochemical Properties and structures of Room Temperature Ionic Liquids. 2. Variation of Alkyl Chain Length in Imidazolium Cation," *Journal of Physical Chemistry,* vol. 109, no. 13, pp. 6103-6110, 2005.

[20] J. A. Widegren, E. M. Saurer, K. N. Marsh and J. W. Magee, "Electrolytic conductivity of four imidazolium-based room-temperature ionic liquids and the effect of a water impurity," *J. Chem. Thermodyn,* vol. 37, no. 6, pp. 569-575, 2005.

[21] R. E. Wirz, A. L. Collins, Z. Chen, C. Huerta, G. Z. Li, S. A. Samples, A. Thuppul, P. L. Wright, N. M. Uchizono, H. Huh, M. J. Davis and A. Ottaviano, "Electric Propulsion Activites at the UCLA Plasma & Space

Propulsion Laboratory," in *IEPC-2019-457, 36th International Electric Propulsion Conference*, Vienna, Austria, 2019.

[22] A. Hayati, A. I. Bailey and T. F. Tadros, "Mechanism of stable jet formation in electrohydrodynamic atomization," *Nature,* vol. 319, pp. 41-43, 1986.

[23] V. Shtern and A. Barrero, "Striking features of fluid flows in Taylor cones related to electrosprays," *Journal of Aerosol Sciences,* vol. 25, no. 6, pp. 1049-1063, 1994.

[24] A. Barrero, A. M. Gañán-Calvo, J. Davila, A. Palacios and E. Gomez-Gonzales, "The Role of the Electrical Conductivity and Viscosity on the Motions inside Taylor Cone," *Journal of Electrostatics,* vol. 47, pp. 13-26, 1999.

[25] R. Nayak, R. Padhye, I. L. Kyratzis, Y. B. Truong and L. Arnold, "Effect of viscosity and electrical conductivity on the morphology and fiber diameter in melt electrospinning of polypropylene," *Textile Research Journal,* vol. 83, no. 6, pp. 606-617, 2013.